

On the Advantage of Coherent LoRa Detection in the Presence of Interference

Orion Afisiadis,* Sitian Li,* Andreas Burg*, and Alexios Balatsoukas-Stimming,†

*Telecommunication Circuits Laboratory, École polytechnique fédérale de Lausanne, Switzerland

†Department of Electrical Engineering, Eindhoven University of Technology, The Netherlands

Email: orion.afisiadis@epfl.ch

Abstract—It has been shown that the coherent detection of LoRa signals only provides marginal gains of around 0.7 dB on the additive white Gaussian noise (AWGN) channel. However, ALOHA-based massive Internet of Things systems, including LoRa, often operate in the interference-limited regime. Therefore, in this work, we examine the performance of the LoRa modulation with coherent detection in the presence of interference from another LoRa user with the same spreading factor. We derive rigorous symbol- and frame error rate expressions as well as bounds and approximations for evaluating the error rates. The error rates predicted by these approximations are compared against error rates found by Monte Carlo simulations and shown to be very accurate. We also compare the performance of LoRa with coherent and non-coherent receivers and we show that the coherent detection of LoRa is significantly more beneficial in interference scenarios than in the presence of only AWGN. For example, we show that coherent detection leads to a 2.5 dB gain over the standard non-coherent detection for a signal-to-interference ratio (SIR) of 3 dB and up to a 10 dB gain for an SIR of 0 dB.

I. INTRODUCTION

LoRaWAN is a proprietary standard, which is currently one of the most popular non-cellular communications solutions for the Internet of Things [1]–[3]. The physical layer of LoRaWAN, which is simply called LoRa [4], uses symbols which are frequency chirps that span the entire allocated bandwidth [5]. The spreading gain of LoRa is determined by the spreading factor (SF), which can be adjusted to trade off data rate and transmission time for range and robustness. For energy efficiency reasons, LoRa uses a non-slotted ALOHA-based MAC protocol. Unfortunately, the long transmission times of LoRa packets along with this ALOHA-based protocol result in a large number of packet collisions [6]–[8]. This issue is aggravated as the number of LoRa devices increases in the future, putting the scalability of LoRa networks at risk as they become interference-limited.

We call this type of LoRa packet collisions *same-technology interference*. On the contrary, interference coming from other technologies in the industrial, scientific and medical (ISM) band is called *cross-technology interference* [9], [10]. Same-technology interference can be divided in two main types: the first type is interference from other LoRa nodes which use different spreading factors, which is called *inter-SF interference*. The second, and most severe type of same-technology interference comes from LoRa nodes transmitting with the

same spreading factor, and is called *same-SF interference*. The impact of same-technology interference of both types has received significant attention in the literature [6], [7], [11]–[25].

The scalability of LoRaWAN networks is evaluated either through mathematical models or using system-level simulations. In particular, in system-level simulators it is possible to tune many important parameters of the network, such as the number of nodes per SF, the total number of nodes in the network, the amount of transmitted data, the duty cycle of the nodes, the transmission power, etc. Such system-level simulation environments are therefore essential tools to provide performance results for different network configurations, including large and heavily-loaded networks. Many system-level LoRaWAN simulators have been proposed in the literature during the last years [7], [15], [26]–[38]. All of these simulators rely on models for the performance characteristics (e.g., frame error rates) of the underlying PHY layer. Today, most of these models are highly simplified, especially when it comes to considering interference. To alleviate this issue, it is essential to provide realistic and detailed PHY performance models, especially when considering new types of modulations or receivers. Detailed PHY performance models are essential tools in a combined PHY/MAC layer approach to realistically evaluate the scalability of LoRaWAN [39].

The number of works that provide rigorous probabilistic models for the performance of LoRa PHY is still relatively small, but growing. The performance of LoRa under additive white Gaussian noise (AWGN) and various fading scenarios has been studied in the literature, both theoretically [40]–[48] and through experimental measurements [28], [49]. Moreover, the error rate of a LoRa receiver under interference from another LoRa user has been thoroughly examined in [20] and [50]. However, to date the error rate of LoRa has mostly been studied for non-coherent detection. Specifically, the performance of coherent LoRa receivers has, to the best of our knowledge, been examined in [41], [44], [51], [52] for the AWGN scenario, and recently in [53] for Rayleigh fading. Very recently, new error rate approximations have been given both for coherent and non-coherent LoRa in [47]. For AWGN channels, coherent LoRa receivers have been shown to yield only a relatively insignificant performance improvement of approximately 0.7 dB over the non-coherent receiver [51]. In

the same work, the authors also investigated additional orthogonal dimensions for LoRa signaling to improve the throughput of LoRa. Since interference scenarios in LoRa networks are very common, and will become even more common in large-scale LoRa deployments in the near future, the analysis of the performance of coherent LoRa receivers under interference is an important topic that is currently missing in the literature.

Contributions: In this work, we propose coherent detection as a simple method for LoRa receivers to significantly improve their resilience against same-SF interference. To demonstrate the potential, we model the performance of coherent LoRa receivers under same-SF interference from another LoRa user and we derive an expression for the symbol error rate (SER). Since this expression is computationally intensive to evaluate in practice, we also derive a corresponding lower bound and an approximation that are based on Q-functions. Furthermore, we extend our analysis to the frame error rate (FER), which is more useful for LoRa system-level simulators. We show that, interestingly, the performance improvement provided by coherent LoRa receivers can potentially be much larger in the case of same-SF interference than the 0.7 dB improvement shown in the literature for the AWGN case. For example, for a signal-to-interference ratio (SIR) of 0 dB the improvement of the coherent over the non-coherent detection is around 10 dB. We finally note that in this work we provide a thorough interference model, which can be considered as an extension of our interference model in [50]. The new extended interference model avoids oversimplifications on the discrete-time baseband equivalent representation of the interfering signal. Furthermore, the interference model includes effects such as the carrier frequency offset (CFO) of the interferer, and provides a more realistic modeling not only for the proposed coherent detection of LoRa, but also for the existing non-coherent detection.

Outline: The remainder of this paper is organized as follows. In Section II, we provide a description of the LoRa modulation and the standard non-coherent detection. Moreover, we discuss coherent LoRa detection for interference scenarios and we summarize the analysis in the existing literature regarding the error rate of coherent LoRa detection under AWGN. In Section III, we extend the analysis to derive the coherent LoRa symbol error rate expression in the presence of interference. In Section IV, we derive lower bounds and an approximation for the coherent LoRa symbol error rate in the presence of interference based on easy-to-evaluate Q-functions. In Section V, we derive the frame error rate expression which is of great practical interest for system-level simulators. Finally, Section VI contains numerical symbol and frame error rate results and Section VII concludes this paper.

II. COHERENT LORA DETECTION

LoRa is a spread-spectrum modulation with typical values for bandwidth $B \in \{125, 250, 500\}$ kHz. Each LoRa symbol consists of $N = 2^{\text{SF}}$ chips and carries SF bits of information, where $\text{SF} \in \{7, \dots, 12\}$. In the discrete-time baseband-equivalent representation, the bandwidth B is split

into N frequency steps. The first chip of a symbol $s \in \mathcal{S}$, where $\mathcal{S} = \{0, \dots, N-1\}$, begins at a baseband frequency of $(\frac{sB}{N} - \frac{B}{2})$. At every chip of the symbol, the frequency increases by $\frac{B}{N}$, until the Nyquist frequency $\frac{B}{2}$ is reached. When this happens, i.e., at chip $n_{\text{fold}} = N - s$, there is a frequency fold to $-\frac{B}{2}$.

As explained in [51], the general discrete-time baseband-equivalent description of a LoRa symbol s can be written in two forms: in the first form [54], the phase of the first chip of a LoRa symbol is symbol-dependent. This form is therefore not directly suited for coherent demodulation. In the second form, as shown in [50], [51], [55], [56], all LoRa symbols start with the same phase. Therefore, only the second form has inter-symbol phase continuity, which has been described in the LoRa patent [4] as a desirable property.

We follow our notation from [50], [55] and write the discrete-time baseband-equivalent description of a LoRa symbol with inter-symbol phase continuity, as

$$x_s[n] = \begin{cases} e^{j2\pi(\frac{1}{2N}(\frac{B}{f_s})^2 n^2 + (\frac{s}{N} - \frac{1}{2})(\frac{B}{f_s})n)}, & n \in \mathcal{S}_1, \\ e^{j2\pi(\frac{1}{2N}(\frac{B}{f_s})^2 n^2 + (\frac{s}{N} - \frac{3}{2})(\frac{B}{f_s})n)}, & n \in \mathcal{S}_2, \end{cases} \quad (1)$$

where $\mathcal{S}_1 = \{0, \dots, n_{\text{fold}} - 1\}$ and $\mathcal{S}_2 = \{n_{\text{fold}}, \dots, N - 1\}$. In the case where the sampling frequency f_s is equal to B , the discrete-time baseband-equivalent description of a LoRa symbol s can be simplified to¹

$$x_s[n] = e^{j2\pi(\frac{n^2}{2N} + (\frac{s}{N} - \frac{1}{2})n)}, \quad n \in \mathcal{S}. \quad (2)$$

When the transmission takes place over an AWGN channel with a given complex-valued channel gain $h \in \mathbb{C}$, the received LoRa symbol is given by

$$y[n] = hx_s[n] + z[n], \quad n \in \mathcal{S}, \quad (3)$$

where $z[n] \sim \mathcal{CN}(0, \sigma^2)$ is complex AWGN with variance $\sigma^2 = \frac{N_0}{2N}$ and N_0 is the single-sided noise power spectral density. The channel has a magnitude and a phase, i.e., $h = |h|e^{j\phi}$, where we assume $|h| = 1$ without loss of generality, so that the signal-to-noise ratio (SNR) is $\frac{1}{N_0}$.

On the receiver side, the first task is called the *dechirping*, which multiplies the received signal by the complex conjugate of a reference signal x_{ref} . A common choice for the reference signal is the LoRa symbol for $s = 0$

$$x_{\text{ref}}[n] = e^{j2\pi(\frac{n^2}{2N} - \frac{n}{2})}, \quad n \in \mathcal{S}. \quad (4)$$

After dechirping, the discrete Fourier transform (DFT) of the signal is computed to obtain $\mathbf{Y} = \text{DFT}(\mathbf{y} \odot \mathbf{x}_{\text{ref}}^*)$, where \odot denotes the Hadamard product, $\mathbf{y} = [y[0] \ \dots \ y[N-1]]$, and $\mathbf{x}_{\text{ref}} = [x_{\text{ref}}[0] \ \dots \ x_{\text{ref}}[N-1]]$. Non-coherent LoRa

¹As explained in [56], the continuous-time LoRa chirp occupies a slightly larger bandwidth than B . As such, using a sampling rate $f_s = B$ in a real transmission introduces some distortion effects due to aliasing. However, as explained in [56], since N is large in LoRa, most of the signal power lies inside B , and therefore, (2) is a good discrete-time baseband-equivalent description of the LoRa signal.

detection is performed by simply selecting the bin index with the largest magnitude

$$\hat{s} = \arg \max_{k \in \mathcal{S}} (|Y_k|), \quad (5)$$

where Y_k denotes the k -th element of \mathbf{Y} .

A. Coherent LoRa Detection: How and Why?

Coherent LoRa detection necessitates a phase rotation of the received signal to compensate for the channel phase rotation. The phase shift ϕ introduced by the transmission channel can be estimated after initial synchronization using the preamble LoRa symbols, according to

$$\hat{\phi} = \arg \left(\sum_{i=1}^{N_{pr}} Y_0^{(i)} \right), \quad (6)$$

where N_{pr} is the number of preamble symbols in the LoRa packet, and $Y_0^{(i)}$ is the first frequency bin of the i -th preamble symbol.

After the compensation of the phase rotation according to $\mathbf{U} = \mathbf{Y}e^{-j\hat{\phi}}$, coherent detection is performed by selecting the bin index with the maximum projection onto the real axis [44], [51], [52]

$$\hat{s} = \arg \max_{k \in \mathcal{S}} (\Re(U_k)). \quad (7)$$

Fig. 1 illustrates the impact of coherent detection for AWGN and with interference, by showing the elements of \mathbf{U} superimposed as vectors in the complex plane. While the desired signal is aligned with the real axis, signal bins containing noise or interference are circularly symmetric. Unfortunately, for AWGN (see Fig. 1a), the large number of noise signal components renders it likely that at least one is aligned well with the signal, a fact that limits the gain from coherent detection. However, in the interference-limited scenario (Fig. 1b), there is only a small number of interference bins that have a significant magnitude and the risk of one of these few aligning with the real axis (which increases the likelihood of an error event) is low.

B. Coherent LoRa Symbol Error Rate Under AWGN

Before proceeding to analyze the SER of coherent detection with interference, it useful to first recapitulate the performance of coherent detection under AWGN.

In an ideal noiseless receiver and under the assumption of perfect sample synchronization, the DFT of the dechirped signal \mathbf{Y} results in a single frequency bin which contains all the signal energy (i.e., a bin that has magnitude N) and all remaining $N - 1$ bins have zero energy. With AWGN present, the distribution of the frequency bin values Y_k for $k \in \mathcal{S}$ is

$$Y_k \sim \begin{cases} \mathcal{CN}(0, 2\sigma^2), & k \in \mathcal{S}/s, \\ \mathcal{CN}(N \cos \phi + jN \sin \phi, 2\sigma^2), & k = s. \end{cases} \quad (9)$$

where s is the transmitted symbol [50]. The channel phase shift ϕ is fixed for each transmission, but is generally uniformly distributed in $[0, 2\pi)$.

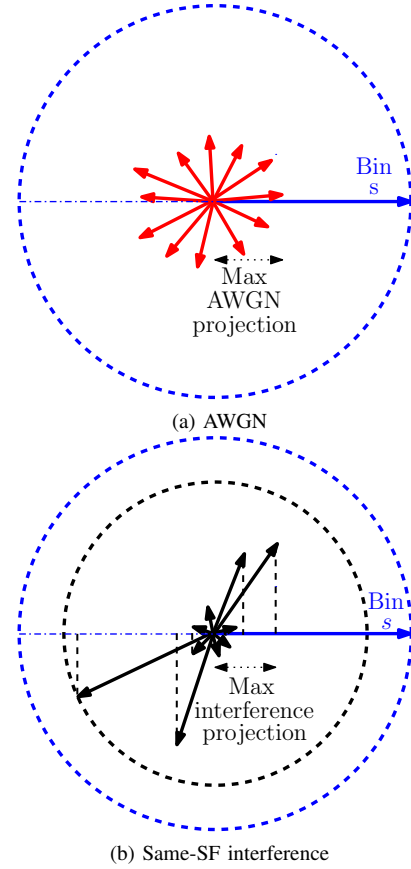


Fig. 1. Illustration of the complex plane representation of the received dechirped signal in frequency domain.

After the compensation for the channel phase by the coherent receiver, the corresponding demodulation metric follows a normal distribution with zero mean for $k \in \mathcal{S}/s$ and a normal distribution with mean N for $k = s$

$$\Re(U_k) \sim \begin{cases} \mathcal{N}(0, \sigma^2), & k \in \mathcal{S}/s, \\ \mathcal{N}(N, \sigma^2), & k = s. \end{cases} \quad (10)$$

A symbol error occurs if and only if any of the $\Re(U_k)$ values for $k \in \mathcal{S}/s$ exceeds the value of $\Re(U_s)$, or, equivalently, if and only if $\Re(U_{\max}) > \Re(U_s)$, where $\Re(U_{\max}) = \max_{k \in \mathcal{S}/s} \Re(U_k)$. The probability density function (PDF) of bin s is $f_{\Re(U_s)}(y) = \mathcal{N}(N, \sigma^2)$ and the cumulative distribution function (CDF) of the maximum projection of the remaining bins on the real axis, $\Re(U_{\max})$, is

$$F_{\Re(U_{\max})}(y) = \left(1 - Q\left(\frac{y}{\sigma}\right) \right)^{N-1}, \quad (11)$$

where $Q(\cdot)$ denotes the Q-function. Therefore, the probability of symbol error for a given transmitted symbol s is

$$P(\hat{s} \neq s|s) = \frac{1}{\sigma\sqrt{2\pi}} \int_{y=0}^{+\infty} \left(1 - \left(1 - Q\left(\frac{y}{\sigma}\right) \right)^{N-1} \right) e^{-\frac{(y-N)^2}{2\sigma^2}} dy. \quad (12)$$

The SER for all symbols s is identical, therefore (12) is also equal to the expected SER $P(\hat{s} \neq s)$.

$$P(\hat{s} \neq s) = \frac{1}{\sigma\sqrt{2\pi}} \sum_{q=1}^{N-1} (-1)^{q+1} \binom{N-1}{q} \int_{y=0}^{+\infty} \left(Q\left(\frac{y}{\sigma}\right)\right)^q e^{-\frac{(y-N)^2}{2\sigma^2}} dy \quad (8)$$

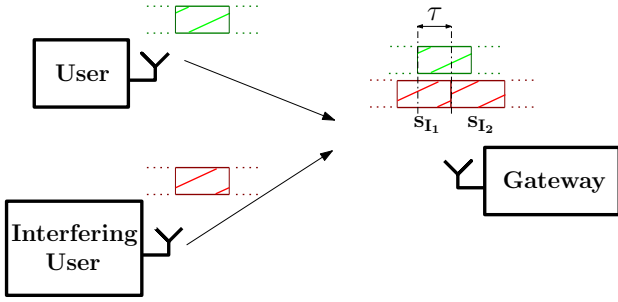


Fig. 2. Illustration of LoRa uplink transmission with one interfering user having an arbitrary τ [50].

The SER in (12) is equivalent to [44, Eq. (17)], where the authors explain how to evaluate it numerically without suffering from numerical problems. The authors of [51] give a low-complexity approximation for the coherent LoRa SER under AWGN. The approximation from [51], which we write below using our notation, was derived using curve fitting

$$P(\hat{s} \neq s) \approx Q\left(\frac{1 - \sqrt{\sigma^2(1.161 + 0.2074 \cdot \text{SF})}}{\sqrt{\sigma^2 + \sigma^2(0.2775 - 0.0153 \cdot \text{SF})}}\right). \quad (13)$$

The approximation in (13) can be evaluated with very low complexity and is very accurate.

As an alternative to the empirical fit in (13), we note here that using Newton's binomial identity, we have

$$1 - \left(1 - Q\left(\frac{y}{\sigma}\right)\right)^{N-1} = \sum_{q=1}^{N-1} (-1)^{q+1} \binom{N-1}{q} \left(Q\left(\frac{y}{\sigma}\right)\right)^q, \quad (14)$$

and thus we can write (12) as (8). The SER written in the form of (8) contains integer powers of the Q-function, and thus it can be evaluated using the simple and tight approximation for the integer powers of the Q-function of [57].

III. COHERENT LORA SYMBOL ERROR RATE UNDER SAME-SF INTERFERENCE

In this section, we extend the signal model of Section II for the same-SF LoRa interference scenario. We then derive the SER expression of LoRa with coherent detection under same-SF interference.

A. Interference Signal Model

Let us consider a LoRa gateway which is perfectly synchronized to the signal of a desired user on which the signal of an interfering user is superimposed. Although the impact of inter-SF interference has been shown to be non-negligible [24], it is quite different than the impact of same-SF interference, due to spreading gain. As a result, the two

types of interference need to be analyzed separately. Due to the approximate orthogonality of different spreading factors, inter-SF interference results in a wide-band spectrum with low spectral density in the frequency domain after dechirping [24]. Therefore, inter-SF interference can be approximately treated as white noise and can be included in our model by properly adjusting the SNR. In this Section we only consider the case where the interfering packet has the same SF as the desired user, which is the most severe type of interference. To simplify the analysis, we consider only one interfering user. If multiple interfering users collide at the same time, the strongest user typically dominates the impact on the error rate.

Since LoRa uses the non-slotted ALOHA protocol for medium access control, the interfering signal $y_I[n] = h_I x_I[n]$ is neither synchronized to the desired user nor to the gateway. However, we assume that the gateway is perfectly synchronized to the desired user, using one of the known synchronization methods [58], [59], as shown in [60]. Moreover, we assume that any carrier frequency offset of the desired user has been perfectly estimated and compensated. However, the gateway can perform CFO estimation and compensation only for one user, therefore, there is no CFO estimation and compensation for the interfering user. Thus, we need to include the CFO of the interferer in order to obtain an accurate model.

As shown in Fig. 2, due to the lack of any time synchronization with the interferer, the interfering signal $x_I[n]$ will generally consist of parts of two distinct LoRa symbols, which we denote by s_{I_1} and s_{I_2} . Following the notation of [50], let τ be the relative time offset between the first chip of the transmitted symbol of interest s and the first chip of the interfering symbol s_{I_2} (i.e., the first chip of the second interfering symbol s_{I_2} starts τ chip durations *after* the first chip of the desired symbol s). We note that the offset τ can be split into an integer part $L = \lfloor \tau \rfloor$, and a non-integer part $\lambda = \tau - \lfloor \tau \rfloor$. We consider that τ has a uniform distribution in $[0, N)$, due to the complete lack of synchronization. The discrete-time baseband equivalent equation² of $x_I[n]$ can be found using (1) for s_{I_1} and s_{I_2} , appropriately adjusted to

²We note that the exact expression for $x_I[n]$, as given by (15), requires the use of (1) for representing each one of the two interfering symbols s_{I_1} and s_{I_2} . In our expression for $x_I[n]$ in [50, Eq. (21)], we instead use (2) for representing s_{I_1} and s_{I_2} . Therefore, [50, Eq. (21)] can only be considered as an approximation of the actual expression for $x_I[n]$ in the presence of non-integer time offsets τ . In [50] we use the aforementioned simplification, but in the current work we present the exact expression for a more realistic analysis.

include the time offset τ

$$x_I[n] = \begin{cases} e^{j2\pi\left(\frac{(n+N-\tau)^2}{2N} + (n+N-\tau)\left(\frac{s_{I_1}}{N} - \frac{1}{2}\right)\right)}, & n \in \mathcal{N}_{L_1}, \\ e^{j2\pi\left(\frac{(n+N-\tau)^2}{2N} + (n+N-\tau)\left(\frac{s_{I_1}}{N} - \frac{3}{2}\right)\right)}, & n \in \mathcal{N}_{L_2}, \\ e^{j2\pi\left(\frac{(n-\tau)^2}{2N} + (n-\tau)\left(\frac{s_{I_2}}{N} - \frac{1}{2}\right)\right)}, & n \in \mathcal{N}_{L_3}, \\ e^{j2\pi\left(\frac{(n-\tau)^2}{2N} + (n-\tau)\left(\frac{s_{I_2}}{N} - \frac{3}{2}\right)\right)}, & n \in \mathcal{N}_{L_4}, \end{cases} \quad (15)$$

where

$$\mathcal{N}_{L_1} = \{0, \dots, \lceil \tau \rceil - s_{I_1} - 1\}, \quad (16)$$

$$\mathcal{N}_{L_2} = \{\max(\lceil \tau \rceil - s_{I_1}, 0), \dots, \lceil \tau \rceil - 1\}, \quad (17)$$

$$\mathcal{N}_{L_3} = \{\lceil \tau \rceil, \dots, \min(N - s_{I_2} + \lceil \tau \rceil - 1, N - 1)\}, \quad (18)$$

$$\mathcal{N}_{L_4} = \{N - s_{I_2} + \lceil \tau \rceil, \dots, N - 1\}, \quad (19)$$

and where we define $\{a, \dots, b\} = \emptyset$ if $b < a$.

Furthermore, let f_{c_I} be the carrier frequency used during up-conversion at the transmitter of the interfering user and f_c be the carrier frequency used during down-conversion at the gateway after alignment with the carrier frequency of the desired user. The carrier frequency offset of the interfering user is the difference $\Delta f_c = f_{c_I} - f_c$, while any frequency offset of the desired user is perfectly compensated. As a result, the corresponding signal model is

$$y[n] = hx[n] + h_I c_I[n] x_I[n] + z[n], \quad n \in \mathcal{S}, \quad (20)$$

where h is the channel gain between the user and the LoRa gateway, $x[n]$ is the transmitted signal, h_I is the channel gain between the interferer and the gateway, $x_I[n]$ is the transmitted interfering signal, $c_I[n] = e^{j2\pi(n+(m-1)N)\frac{\Delta f_c}{f_s}}$ is the CFO term affecting the m -th symbol in the interfering packet, and $z[n] \sim \mathcal{N}(0, \sigma^2)$ is AWGN. We note that, after despreading, the CFO translates into a time offset $\tau_{\text{cfo}} = \frac{\Delta f_c N}{f_s}$ [46], and similarly to τ , the offset τ_{cfo} can be split into an integer part $L_{\text{cfo}} = \lfloor \tau_{\text{cfo}} \rfloor$, and a non-integer part $\lambda_{\text{cfo}} = \tau_{\text{cfo}} - \lfloor \tau_{\text{cfo}} \rfloor$. Since $|h| = 1$, the signal-to-interference ratio (SIR) can be defined as $\text{SIR} = \frac{1}{P_I}$, where $P_I = |h_I|^2$ is the received power of the interfering user at the gateway. The demodulation of $y[n]$ at the receiver yields

$$\begin{aligned} \mathbf{Y} &= \text{DFT}(h\mathbf{x} \odot \mathbf{x}_{\text{ref}}^*) + \text{DFT}(h_I \mathbf{c}_I \odot \mathbf{x}_I \odot \mathbf{x}_{\text{ref}}^*) \\ &+ \text{DFT}(\mathbf{z} \odot \mathbf{x}_{\text{ref}}^*). \end{aligned} \quad (21)$$

We call $\text{DFT}(h_I \mathbf{c}_I \odot \mathbf{x}_I \odot \mathbf{x}_{\text{ref}}^*) = \text{DFT}(\mathbf{y}_I \odot \mathbf{x}_{\text{ref}}^*)$ the *received interference pattern*. The received interference pattern depends on the time-domain interference signal \mathbf{y}_I , which is in turn a function of the interfering symbols s_{I_1}, s_{I_2} , the channel h_I , the interferer time offset τ , and the CFO between the interferer and the gateway.

We note that, in the presence of a fractional CFO, the received interference pattern is not just a scaled version of the pattern without CFO, but it has a different shape. A LoRa signal model in the presence of both time and frequency offsets has first been discussed in [59] for the LoRa preamble. An

example of a received interference pattern with CFO is shown in Fig. 3. In Fig. 3a, we show the magnitude of the interference pattern across different bins after the DFT, while Fig. 3b shows also the phase in the complex plane. In coherent detection of LoRa, the received interference pattern has to be examined on the complex plane, since the symbol decision is performed after projection on the real axis instead of based only on the magnitude as in [50].

B. Symbol Error Rate Under Same-SF Interference

With the above described signal and interference model, we can now derive the SER expression following an approach that is similar to [50].

1) *Distribution of the Decision Metric*: Let R_k be the value of the received interference pattern at frequency bin k . For a specific combination of a symbol s and an interference pattern \mathbf{y}_I , the distribution of Y_k is

$$Y_k \sim \begin{cases} \mathcal{CN}(|R_k| \cos \theta_k + j|R_k| \sin \theta_k, 2\sigma^2), & k \in \mathcal{S}/s \\ \mathcal{CN}(N \cos \phi + |R_k| \cos \theta_k + \\ + j(N \sin \phi + |R_k| \sin \theta_k), 2\sigma^2), & k = s, \end{cases}$$

where $\theta_k = \theta + \theta_{I_k}$ is the phase shift for bin k introduced by the interference channel and by the CFO. We note that θ is fixed for all symbols in a given packet, but changes for different packet transmissions, and is generally uniformly distributed in $[0, 2\pi)$. However, the phase offset induced by the CFO of the interferer, θ_{I_k} , is deterministic, but different for each bin k , and changes for each symbol in a packet. Since the received signal \mathbf{U} is rotated by $-\phi$ due to the coherent detection, we define the phase shift between the interferer and the user as $\omega_k = \omega + \theta_{I_k}$, where $\omega = \theta - \phi$, which corresponds to relative phase shift of the interferer, after the rotation introduced by the coherent receiver. We note that since ϕ is fixed for each transmission, but generally uniformly distributed in $[0, 2\pi)$, it holds that ω , is also fixed for each transmission, but generally uniformly distributed in $[0, 2\pi)$.

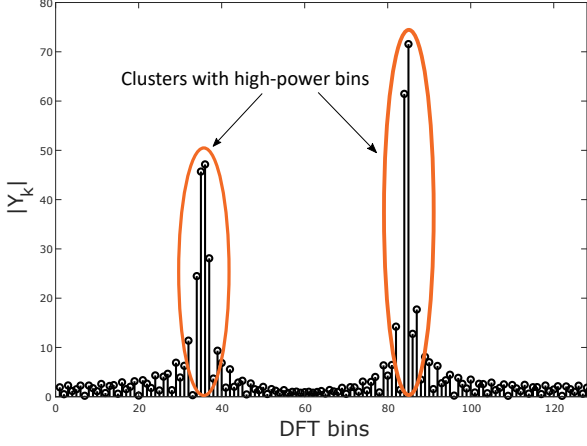
The demodulation metric $\Re(U_k)$ in the presence of interference, is therefore distributed as

$$\Re(U_k) \sim \begin{cases} \mathcal{N}(|R_k| \cos \omega_k, \sigma^2), & k \in \mathcal{S}/s \\ \mathcal{N}(N + |R_k| \cos \omega_k, \sigma^2), & k = s. \end{cases} \quad (23)$$

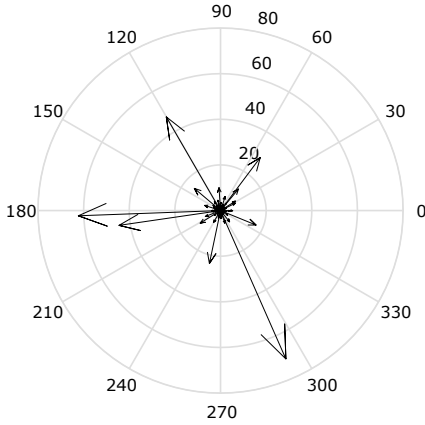
2) *Symbol Error Rate Expression*: For a given realization of a transmission, conditioning on both the phase ϕ of the channel of the desired user and the phase θ of the channel of the interfering user, can be replaced by conditioning on $\omega = \theta - \phi$. For notation simplicity, we denote the SER for a given symbol s , conditioned on s_{I_1}, s_{I_2} , the relative offset τ , the equivalent offset due to the CFO τ_{cfo} , and the phase difference ω , as $P(\hat{s} \neq s | s, s_{I_1}, s_{I_2}, \tau, \tau_{\text{cfo}}, \omega) = P(\hat{s} \neq s | s, \mathbf{y}_I, \omega)$. This error probability can be written as

$$P(\hat{s} \neq s | s, \mathbf{y}_I, \omega) = 1 - \frac{1}{\sigma\sqrt{2\pi}} \int_{y=0}^{+\infty} e^{-\frac{(y-\mu_s)^2}{2\sigma^2}} F_{\Re(U_{\text{max}})}(y) dy, \quad (24)$$

$$P(\hat{s} \neq s | \tau_{\text{cfo}}) = 1 - \frac{1}{\sigma(2\pi)^{\frac{3}{2}}} \sum_{s=0}^{N-1} \sum_{s_{I_1}=0}^{N-1} \sum_{s_{I_2}=0}^{N-1} \int_{\tau=0}^N \int_{\omega=0}^{2\pi} \int_{y=0}^{+\infty} e^{-\frac{(y-\mu_s)^2}{2\sigma^2}} \prod_{\substack{k=1 \\ k \neq s}}^N F_{\mathcal{N}}(y; \mu_k, \sigma^2) dy d\omega d\tau \quad (22)$$



(a) The magnitude of the received interference pattern



(b) The complex plane representation of the received interference pattern

Fig. 3. The received interference pattern for SF = 7, $s_{I_1} = 83$, $s_{I_2} = 4$, $\tau = 88.4$, $|h_I| = 1$, and $\lambda_{\text{cfo}} = 0.4$.

where $\mu_s = N + |R_s| \cos \omega_s$, and $F_{\mathcal{R}(U_{\text{max}})}(y) = \prod_{\substack{k=1 \\ k \neq s}}^N F_{\mathcal{N}}(y; \mu_k, \sigma^2)$, where $F_{\mathcal{N}}(y; \mu_k, \sigma^2)$ denotes the CDF of a Gaussian distribution, and where $\mu_k = |R_k| \cos \omega_k$. Following a similar reasoning as in [50] for the non-coherent receiver, the full expression for $P(\hat{s} \neq s | \tau_{\text{cfo}})$ in the case of a coherent receiver, conditioned only on the CFO value, is given in (22).

IV. SYMBOL ERROR RATE BOUND AND APPROXIMATION

Unfortunately, the computational complexity for evaluating the expression in (22) is prohibitive and numerical problems may also arise. Therefore, in this section, we derive a lower

bound as well as an approximation based on this bound for efficiently evaluating (22) in the practically relevant SNR operating regime of LoRa.

A. Interference Patterns

Let V_k be the value of the received interference pattern at frequency bin k after the rotation due to the coherent receiver, i.e., $V_k = e^{-j\phi} R_k$, assuming perfect knowledge of ϕ . We first derive an explicit form for the real-axis projection of V_k , i.e., $\Re(V_k)$, $k \in \mathcal{S}$. Using the definition of the DFT and after some simple algebraic transformations, we obtain

$$\Re(V_k) = |h_I| \sum_{j=1}^4 A_{k,j} \cos \theta_{k,j}, \quad (25)$$

where $A_{k,j}$ and $\theta_{k,j}$ are given in the Appendix.

B. Symbol Error Rate Bound

We now wish to derive a bound for $P(\hat{s} \neq s | \tau_{\text{cfo}})$, with the use of Q-functions, that can be evaluated more efficiently than (22). First, we assume that the maximum of $\Re(V_k)$, as depicted in Fig. 1b, dominates the interference-induced SER. In particular, taking into consideration only the interfering bin with the maximum projection results in a lower bound for the probability of error. We need to search over all $N-1$ possible erroneous bins in order to evaluate the maximum projection

$$V_{k_{\text{max}}} = \max_{k \in \mathcal{S}/s} (\Re(V_k)). \quad (28)$$

The decision metric for the bin of the maximum projection is Gaussian distributed with mean $V_{k_{\text{max}}}$ and variance σ^2 , while the decision metric for the desired bin s is Gaussian distributed with mean $N + \Re(V_s)$ and variance σ^2 . Therefore, their difference also follows a Gaussian distribution with mean $V_{k_{\text{max}}} - N - \Re(V_s)$ and variance $2\sigma^2$, and a symbol error happens if this difference is positive. Thus, for a given transmitted symbol s , a particular realization of the user channel, and a particular realization of the interference pattern, i.e., for given s , s_{I_1} , s_{I_2} , τ , τ_{cfo} , and ω , the probability that the interfering bin has higher energy than bin s can be bounded from below by

$$P(\hat{s} \neq s | s, \mathbf{y}_I, \omega) \geq Q\left(\frac{N + \Re(V_s) - V_{k_{\text{max}}}}{\sqrt{2\sigma^2}}\right), \quad (29)$$

where $\Re(V_s)$ is the projection of the interference which lies on top of our desired symbol on bin s . Since symbol s can take any of the N possible values, the error rate after removing the conditioning on s can be written as

$$P(\hat{s} \neq s | \mathbf{y}_I, \omega) \geq \frac{1}{N} \sum_{s=0}^{N-1} Q\left(\frac{N + \Re(V_s) - V_{k_{\text{max}}}}{\sqrt{2\sigma^2}}\right). \quad (30)$$

$$\mathcal{D}_1 = \left\{ \left[N - \lfloor \tau - \tau_{\text{cfo}} \rfloor + s_{I_1} - \frac{K-1}{2} \right]_N, \dots, \left[N - \lfloor \tau - \tau_{\text{cfo}} \rfloor + s_{I_1} + \frac{K-1}{2} \right]_N \right\} \quad (26)$$

$$\mathcal{D}_2 = \left\{ \left[N - \lfloor \tau - \tau_{\text{cfo}} \rfloor + s_{I_2} - \frac{K-1}{2} \right]_N, \dots, \left[N - \lfloor \tau - \tau_{\text{cfo}} \rfloor + s_{I_2} + \frac{K-1}{2} \right]_N \right\} \quad (27)$$

Using (30), we can finally bound from below the interference-induced SER as

$$P(\hat{s} \neq s | \tau_{\text{cfo}}) = \frac{2\pi}{N^3} \sum_{s_{I_1}=0}^{N-1} \sum_{s_{I_2}=0}^{N-1} \int_0^{2\pi} \int_0^N P(\hat{s} \neq s | \mathbf{y}_I, \omega) d\tau d\omega. \quad (31)$$

We can further reduce the complexity for evaluating the interference-induced SER in (31) by reducing the complexity of evaluating $P(\hat{s} \neq s | \mathbf{y}_I, \omega)$ using a less tight lower bound. Looking at (39)–(42) in the Appendix, we observe that the DFT bins adjacent to bins $N - \lfloor \tau - \tau_{\text{cfo}} \rfloor + s_{I_1}$ and $N - \lfloor \tau - \tau_{\text{cfo}} \rfloor + s_{I_2}$ have considerably higher energy, compared to the rest of the bins, due to the combination of the fractional part of the misalignment and the fractional part of the CFO. An example of this can be observed in Fig. 3a.

Let K define the number of most relevant bins in each cluster of high-power DFT bins, as depicted in Fig. 3a. Let $\mathcal{D} = \mathcal{D}_1 \cup \mathcal{D}_2$, with \mathcal{D}_1 and \mathcal{D}_2 given by (26)–(27), where $|\mathcal{D}| = 2K$. \mathcal{D}_1 and \mathcal{D}_2 are the sets of K most relevant bins in the cluster around $N - \lfloor \tau - \tau_{\text{cfo}} \rfloor + s_{I_1}$ and of K most relevant bins in the cluster around $N - \lfloor \tau - \tau_{\text{cfo}} \rfloor + s_{I_2}$, respectively, where we denote $[x]_y = x \bmod y$. We note here that the two sets \mathcal{D}_1 and \mathcal{D}_2 of the most relevant bins can have overlapping bins. We are interested in treating the set of most relevant bins $\mathcal{D} = \mathcal{D}_1 \cup \mathcal{D}_2$ separately from the rest of the bins. As can be seen in Fig. 3b and Fig. 1b, there is a high probability that the maximum projection $V_{k_{\text{max}}}$ will occur due to one of these most relevant bins that belong to \mathcal{D} . Increasing K (i.e., increasing also the cardinality of the set \mathcal{D}) increases the number of cases in which the bin with the maximum projection will be included in the set \mathcal{D} . We reduce the set of bins we consider from \mathcal{S} with cardinality $|\mathcal{S}| = N$, to \mathcal{D} with much smaller cardinality $|\mathcal{D}| \ll N$ which does not explicitly scale with SF. This way the search in equation (28) is only conducted over \mathcal{D} , instead of \mathcal{S} as

$$V_{k_{\text{max}}} = \max_{k \in \mathcal{D}/s} (\Re(V_k)). \quad (32)$$

By using (32) instead of (28) in (30), we obtain a lower bound which can be evaluated with lower complexity.

C. Symbol Error Rate Approximation

We now wish to derive an approximation for $P(\hat{s} \neq s | \tau_{\text{cfo}})$ that can be evaluated with even less computational complexity than (30)–(31).

The impact of the interference at bin s is significant only when $s \in \mathcal{D}$. For all cases where $s \notin \mathcal{D}$ the impact of the interference at bin s is negligible even if it aligns with the real axis. By distinguishing the N bins in two sets, namely

set \mathcal{D} where we account for the interference impact at bin s , and set \mathcal{S}/\mathcal{D} where we do *not* account for the interference impact at bin s , (30) can be approximated as

$$P(\hat{s} \neq s | \mathbf{y}_I, \omega) \approx \frac{1}{N} \left(\sum_{s \in \mathcal{D}} Q \left(\frac{N + \Re(V_s) - V_{k_{\text{max}}}}{\sqrt{2\sigma^2}} \right) + (N - |\mathcal{D}|) Q \left(\frac{N - V_{k_{\text{max}}}}{\sqrt{2\sigma^2}} \right) \right). \quad (33)$$

Using (33), $P(\hat{s} \neq s | \mathbf{y}_I, \omega)$ only requires the evaluation of $|\mathcal{D}| + 1$ Q-functions, instead of N Q-functions needed for (30), which again is specifically advantageous for large SFs (corresponding to large N). We show in the results, that choosing a very small K , e.g., $K = 5$, i.e., $|\mathcal{D}| = 10$, is sufficient for accurate results, for all examined SFs. Finally, the approximation in (33) can be replaced directly in (31).

The integral over the offset τ in (31) can be evaluated numerically by discretizing the interval $[0, N)$ with a step size ϵ . Moreover, the integral over ω can be evaluated by discretizing the interval $[0, 2\pi)$ with a step size ρ . In the results, we show that a discretization step size choice of $\epsilon = \frac{1}{5}$ and $\rho = \frac{\pi}{2}$ provides a low-complexity, yet accurate, evaluation of (31).

In the AWGN-limited regime (i.e., at low SNR), the above approximation eventually becomes inaccurate, since all bins have similar values and no single bin projection dominates the error rate. To fix this issue, let $P^{(N)}(\hat{s} \neq s)$ denote the SER under AWGN given in (12), which can be efficiently evaluated using the approximation in (13), and let $P^{(I)}(\hat{s} \neq s | \tau_{\text{cfo}})$ be the interference-driven SER from (31). Then, a final estimate of the average SER that is accurate also in the low-SNR regime can be approximated by

$$P(\hat{s} \neq s | \tau_{\text{cfo}}) \approx P^{(N)}(\hat{s} \neq s) + \left(1 - P^{(N)}(\hat{s} \neq s) \right) P^{(I)}(\hat{s} \neq s | \tau_{\text{cfo}}). \quad (34)$$

V. COHERENT LORA FRAME ERROR RATE UNDER SAME-SF INTERFERENCE

In system-level simulator environments the FER is generally of greater practical interest than the SER, because system-level simulators, typically take decisions on a frame-by-frame basis. Therefore, in this section we derive expressions to calculate the FER of a coherent uncoded LoRa system. These expression can be used for the LoRa modes that use channel codes of rates $4/5$, and $4/6$, which have error-detection, but no error-correction capabilities, as well as for the uncoded mode. The extension of the analysis to a coded LoRa system can be done following the methodology of [46].

$$P(\hat{\mathbf{s}} \neq \mathbf{s} | F_I, \tau_{\text{cfo}}) = \frac{1}{N} \int_0^N \left(1 - (1 - P(\hat{\mathbf{s}} \neq \mathbf{s} | \tau, \tau_{\text{cfo}}))^{F_I} \left(1 - P^{(N)}(\hat{\mathbf{s}} \neq \mathbf{s}) \right)^{F - F_I} \right) d\tau \quad (35)$$

1) *FER for the overlapping portion of the packets:* We assume perfect frame synchronization for the desired user, even under the impact of interference. Generally, due to the time offset between the desired and the interfering frame, only part of the desired frame is affected by interference. In the following, we consider only the part of the frame that is affected by interference. This way, our derived expression is a straightforward basis for computing FERs for any partial collision of two frames by splitting the frame under consideration into a collision interval which is affected by interference and a second part that is affected only by AWGN. The averaging over all possible relative positions of the packets through Monte Carlo simulations is then inherently done by the network simulator itself.

A collision interval of F LoRa symbols is denoted by the vector \mathbf{s} and the corresponding estimated symbols at the receiver are denoted by the vector $\hat{\mathbf{s}}$. The FER is therefore $P(\hat{\mathbf{s}} \neq \mathbf{s})$. We note that the expression for the SER derived in Section III can not be used as is for the evaluation of the FER because it includes an expectation over the random variables τ and ω , while all symbols in a frame experience the same τ and the same ω over the course of the frame. However, the CFO of the interferer results in a continuous rotation of the samples in the interfering packet. Therefore, for sufficiently long frames, we consider the phase of each symbol (as determined by the CFO) as random and allow the expectation over ω to be included on a symbol level. The frame error rate $P(\hat{\mathbf{s}} \neq \mathbf{s})$ can thus be expressed as

$$P(\hat{\mathbf{s}} \neq \mathbf{s} | \tau_{\text{cfo}}) = \frac{1}{N} \int_0^N \left(1 - (1 - P(\hat{\mathbf{s}} \neq \mathbf{s} | \tau, \tau_{\text{cfo}}))^F \right) d\tau. \quad (36)$$

where $P(\hat{\mathbf{s}} \neq \mathbf{s} | \tau, \tau_{\text{cfo}})$ is

$$P(\hat{\mathbf{s}} \neq \mathbf{s} | \tau, \tau_{\text{cfo}}) = \frac{2\pi}{N^2} \sum_{s_{I_1}=0}^{N-1} \sum_{s_{I_2}=0}^{N-1} \int_0^{2\pi} P(\hat{\mathbf{s}} \neq \mathbf{s} | \mathbf{y}_I, \omega) d\omega. \quad (37)$$

The frame error rate in (36) can be considered as an exact expression if we evaluate (37) using (24) (after taking the expectation over s), or as a lower bound if we evaluate (37) using (30), or as an approximation if we evaluate (37) using (33).

2) *Average FER over different overlapping portions of the packets:* In the following, we also present an expression for the average FER over all possible relative positions of the colliding packets. This expression is useful in cases where the averaging over all possible relative positions of the packets is *not* inherently done by a network simulator. To this end, we consider that the interfering frame has the same length as the desired frame. This assumption is taken only for clarity of

the presentation and does not prevent the generalization of the results to any interfering frame length. The difference to (36) is that, due to the time offset between the frames, only part of the frame of interest is affected by interference, and an average of all collision intervals is considered.

As in [50], let $F_I \in \{1, \dots, F\}$, denote the number of symbols in the frame that are affected by the interfering frame. The value of F_I depends on the relative position of the two frames. For the average FER, we consider the expectation over all the possible relative positions of the two frames. We note that, except in the case of perfect alignment between the frame of interest and the interference, there always exists one symbol that is only partially affected by interference. Similarly to [50], we consider the partially-affected symbol as fully-affected by interference, thus including it in F_I . The frame error rate is now given by (35) where $P(\hat{\mathbf{s}} \neq \mathbf{s} | \tau, \tau_{\text{cfo}})$ is given by (37), and $P^{(N)}(\hat{\mathbf{s}} \neq \mathbf{s})$ is the SER under AWGN given in (12) (which can be evaluated efficiently using the approximation in (13)).

Finally, we take the expectation over all possible values of F_I and we obtain the final expression for the average FER over different collision intervals

$$P_{\text{av}}(\hat{\mathbf{s}} \neq \mathbf{s} | \tau_{\text{cfo}}) \approx \frac{1}{F} \sum_{F_I=1}^F P(\hat{\mathbf{s}} \neq \mathbf{s} | F_I, \tau_{\text{cfo}}). \quad (38)$$

VI. RESULTS

In this section, we provide numerical results for the SER and the FER of a coherent LoRa receiver with same-SF interference. We compare the performance against the non-coherent receiver under the same interference conditions. Moreover, we compare the derived approximations against Monte Carlo simulations to show their accuracy. We note that for the Monte Carlo simulations, the interferer time offset τ is simulated by oversampling (1) to create an accurate interference signal, concatenating the oversampled symbols, applying the appropriate offset, and downsampling the received signal to obtain $N = 2^{\text{SF}}$ samples for \mathbf{x}_I .

A. Error Rates

In Fig. 4, we show the results for the FER of a LoRa receiver for SF = 7, for a packet of length $F = 20$ LoRa symbols, under the effect of same-SF interference with an SIR of 0 dB, for $\lambda_{\text{cfo}} \in \{0, 0.5\}$, and for both a coherent and a non-coherent receiver. Results of both our model of (36) (black dotted lines), where we evaluate (37) using the approximation in (33), and of the Monte Carlo simulation (colored lines) are shown. We can see that the curves derived in our analysis match the Monte Carlo simulation curves very well, showing the accuracy of the corresponding approximations. We observe that both for the coherent and the standard non-coherent receiver, the fractional CFO of the interferer has a significant impact on the error

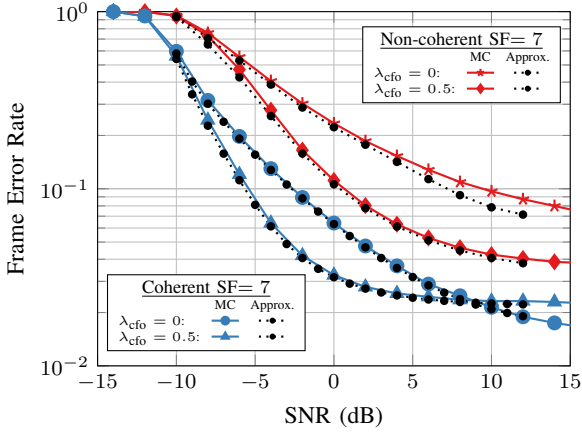


Fig. 4. Frame error rate of the coherent and non-coherent receiver for two different values of CFO, and a packet of length $F = 20$ LoRa symbols under AWGN and same-SF interference for $SF = 7$ and $P_I = 0$ dB.

rate. It is interesting to see that for lower values of SNR the fractional CFO of the interferer is beneficial for the error rate, but at high SNRs an interferer with a higher fractional CFO value results in a higher error floor. We note that the same behavior appears also for the non-coherent receiver, but at higher SNRs.

In Fig. 5, we show the same results as in Fig. 4, but for an SIR of 3 dB. We note that the general trend of the curves is similar to the trend in Fig. 4. However, we note that the results for SIR = 3 dB show a slightly smaller (but still significant) impact of the CFO of the interferer on the error rate compared to the SIR = 0 dB case depicted in Fig. 4. We conclude that, since the CFO of the interferer is always present, it needs to be included in the model in order to examine its impact, which is not negligible. The inclusion of the CFO of the interferer in the model, and the discussion on its impact on the error rate of both coherent and non-coherent receivers, is more realistic than the model in [50] for non-coherent receivers, where the CFO of the interferer was not included.

In Fig. 6, we show the results of a Monte Carlo simulation for the SER of a LoRa user for $SF \in \{7, 9, 11\}$ and for an SIR of 3 dB, using the coherent receiver described in this work, as well as the non-coherent receiver described in [50]. The corresponding analytical approximations for the coherent and non-coherent receivers are shown as well. We observe that the coherent receiver has a significant performance gain of up to 2.5 dB for some SNR values compared to the non-coherent receiver. In [44], [51], [52], for the AWGN-only case, a difference of around 0.7 dB was shown between the coherent and the non-coherent receiver. It is, therefore, very interesting to see that using a coherent receiver seems to be much more beneficial under same-SF interference than in the AWGN-only case. Finally, we observe that the low-complexity SER expression in (31), using the approximation in (33), with $|\mathcal{D}| = 10$ and discretization steps $\rho = \frac{\pi}{2}$ and $\epsilon = \frac{1}{5}$ is already very accurate.

In Fig. 7, we show the results of a Monte Carlo simulation

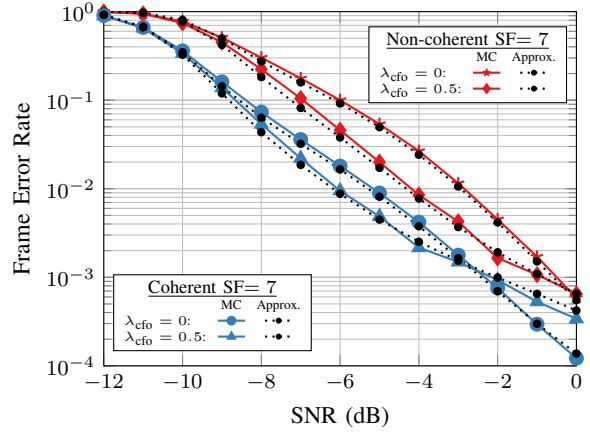


Fig. 5. Frame error rate of the coherent and non-coherent receiver for two different values of CFO, and a packet of length $F = 20$ LoRa symbols under AWGN and same-SF interference for $SF = 7$ and $P_I = -3$ dB.

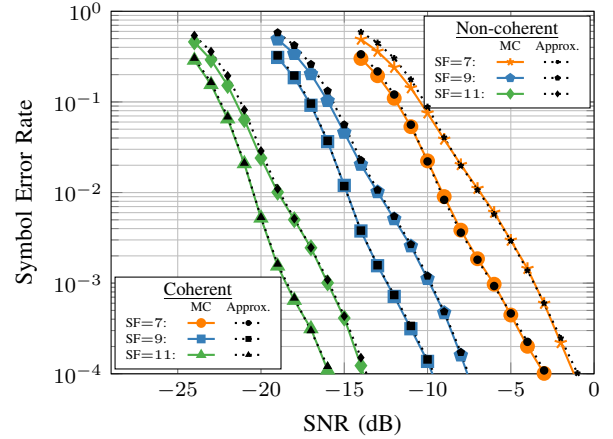


Fig. 6. Symbol error rate of the coherent and non-coherent LoRa receiver under AWGN and same-SF interference for $SF \in \{7, 9, 11\}$ and $P_I = -3$ dB. The approximations for the coherent and the non-coherent case are shown with black dotted lines.

for the FER of both a coherent and a non-coherent LoRa receiver with $SF \in \{7, 9, 11\}$, as well as the corresponding approximation described in Section V. The frame length is $F = 20$ LoRa symbols and the SIR is 3 dB. We observe the same performance difference between the coherent and non-coherent receivers as in the SER curves. Furthermore, we see that the low-complexity approximation for the FER under same-SF interference, described in Section V, is also very accurate.

In Fig. 8, we show the required SNR for $SF = 7$ with a target FER performance of 10^{-1} , for different SIR levels. We show results for both the coherent and the non-coherent receiver for frames of 20 LoRa symbols. As expected, for both receivers, there is an increase in the required SNR to obtain the same FER, as the interference power increases. For the chosen target FER of 10^{-1} we can observe that the coherent receiver requires a much lower increase in the required SNR

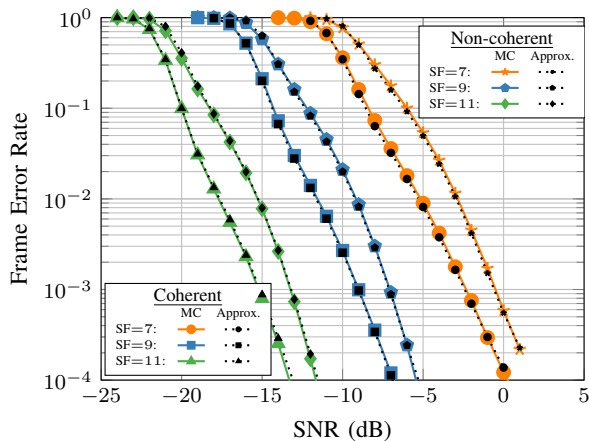


Fig. 7. Frame error rate of the coherent and non-coherent receiver for a packet of length $F = 20$ LoRa symbols under AWGN and same-SF interference for $SF \in \{7, 9, 11\}$ and $P_I = -3$ dB. The approximations for the coherent and the non-coherent case are shown with black dotted lines.

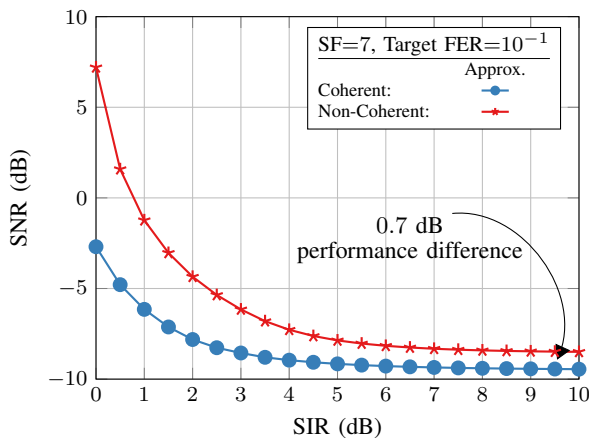


Fig. 8. Required SNR for a target frame error rate of 10^{-1} as a function of the SIR for a packet length of $F = 20$ LoRa symbols for $SF = 7$ for coherent and non-coherent receiver.

compared to the non-coherent receiver. We can also clearly observe that the 0.7 dB performance difference between the coherent and non-coherent receiver reported in [44], [51], [52] for the AWGN case (i.e., for large SIR) is only the smallest possible performance difference. In fact, the coherent receiver is of increasingly greater importance for increasing levels of interference.

B. Phase estimation errors

For coherent detection, a receiver needs to estimate the phase of the received symbols. Although the initial estimation of the phase is easy to do in a LoRa packet, thanks to the preamble, the continuous phase tracking, needed due to the phase drift, cannot be perfect. The phase estimation error due to the imperfect tracking can be modeled as a Gaussian process with variance σ_{tr}^2 , which depends on the phase-drift levels and the quality of the tracking algorithm.

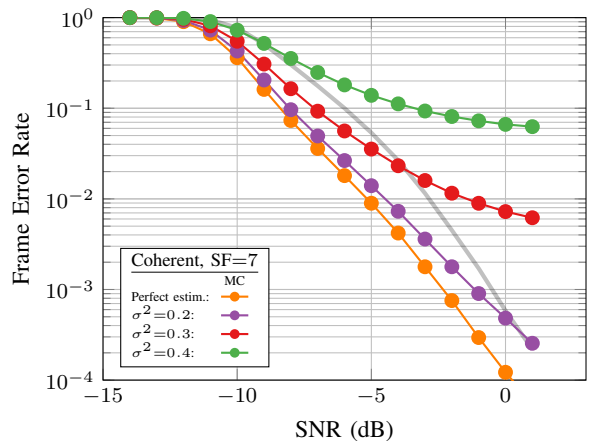


Fig. 9. Frame error rate of the coherent receiver under AWGN and same-SF interference with perfect estimation, and for estimation error $\sigma^2 \in \{0.2, 0.3, 0.4\}$. The packet length is $F = 20$ LoRa symbols, $SF=7$ and $P_I = -3$ dB. The performance of the non-coherent receiver is shown in thick transparent line.

In Fig. 9, we show the performance degradation of a coherent LoRa receiver for three different estimation error variances, $\sigma^2 \in \{0.2, 0.3, 0.4\}$, as well as for perfect phase estimation. The frame length is $F = 20$ LoRa symbols, the spreading factor is $SF = 7$, and $SIR = 3$ dB. The results are compared to the non-coherent receiver, shown in a thick gray line. We observe that the tracking phase-estimation error plays a significant role in the performance of a coherent receiver. With small estimation errors, the coherent receiver can still be competitive to the non-coherent receiver. However, for a coherent receiver to be worth applying compared to a non-coherent receiver, a careful design of the phase-tracking algorithm is needed.

VII. CONCLUSION

In this work we model and investigate the performance of coherent LoRa receivers under same-SF interference. We derive very accurate error rate expressions for the symbol error rate and the frame error rate and we show that the performance improvement of 0.7 dB reported previously for the coherent receiver compared to the non-coherent receiver in the AWGN scenario, is only the smallest possible benefit. The benefit of employing a coherent LoRa receiver increases for higher levels of interference and can reach values close to 10 dB for an SIR of 0 dB. This observation renders coherent LoRa receivers particularly attractive for congested LoRa networks with a high probability of same-SF packet collisions.

ACKNOWLEDGMENT

The authors thank Mathieu Khonneux for helpful discussions on the LoRa signal model in presence of both sampling time offsets and carrier frequency offsets.

APPENDIX

The terms $A_{k,j}$ and $\theta_{k,j}$, for $j \in \{1, \dots, 4\}$, in (25) are

$$A_{k,1} = \frac{\sin\left(\frac{\pi}{N}(s_{I_1} - k - \tau + \tau_{\text{cfo}}) \max([\tau] - s_{I_1}, 0)\right)}{\sin\left(\frac{\pi}{N}(s_{I_1} - k - \tau + \tau_{\text{cfo}})\right)}, \quad (39)$$

$$A_{k,2} = \frac{\sin\left(\frac{\pi}{N}(s_{I_1} - k - \tau + \tau_{\text{cfo}}) ([\tau] - \max([\tau] - s_{I_1}, 0))\right)}{\sin\left(\frac{\pi}{N}(s_{I_1} - k - \tau + \tau_{\text{cfo}})\right)}, \quad (40)$$

$$A_{k,3} = \frac{\sin\left(\frac{\pi}{N}(s_{I_2} - k - \tau + \tau_{\text{cfo}}) (\min(N - s_{I_2} + [\tau], N) - [\tau])\right)}{\sin\left(\frac{\pi}{N}(s_{I_2} - k - \tau + \tau_{\text{cfo}})\right)}, \quad (41)$$

$$A_{k,4} = \frac{\sin\left(\frac{\pi}{N}(s_{I_2} - k - \tau + \tau_{\text{cfo}}) \max(s_{I_2} - [\tau], 0)\right)}{\sin\left(\frac{\pi}{N}(s_{I_2} - k - \tau + \tau_{\text{cfo}})\right)}, \quad (42)$$

and

$$\theta_{k,1} = \frac{\pi}{N} \left(-\tau^2 + \tau N + s_{I_1} (2\tau - [\tau] + s_{I_1} + 1) + (k + \tau - \tau_{\text{cfo}}) ([\tau] - s_{I_1} - 1) - 2N(m-1)\tau_{\text{cfo}} - \omega \frac{N}{\pi} \right), \quad (43)$$

$$\theta_{k,2} = \frac{\pi}{N} \left(-\tau^2 - \tau N + s_{I_1} (2\tau - [\tau] + \max([\tau] - s_{I_1}, 0) + 1) + (k + \tau - \tau_{\text{cfo}}) ([\tau] + \max([\tau] - s_{I_1}, 0) - 1) - 2N(m-1)\tau_{\text{cfo}} - \omega \frac{N}{\pi} \right), \quad (44)$$

$$\theta_{k,3} = \frac{\pi}{N} \left(-\tau^2 - \tau N + s_{I_2} (2\tau - \min(N - s_{I_2} + [\tau], N) + [\tau] + 1) + (k + \tau - \tau_{\text{cfo}}) (\min(N - s_{I_2} + [\tau], N) - [\tau] - 1) - 2N(m-1)\tau_{\text{cfo}} - \omega \frac{N}{\pi} \right), \quad (45)$$

$$\theta_{k,4} = \frac{\pi}{N} \left(-\tau^2 - 3\tau N + s_{I_2} (2\tau - 2N + s_{I_2} - [\tau] + 1) + (k + \tau - \tau_{\text{cfo}}) (2N - s_{I_2} + [\tau] - 1) - 2N(m-1)\tau_{\text{cfo}} - \omega \frac{N}{\pi} \right). \quad (46)$$

REFERENCES

- [1] U. Raza, P. Kulkarni, and M. Sooriyabandara, "Low power wide area networks: An overview," *IEEE Communications Surveys & Tutorials*, vol. 19, no. 2, pp. 855–873, Secondquarter 2017.
- [2] J. Haxhibeqiri, E. De Poorter, I. Moerman, and J. Hoebeke, "A survey of LoRaWAN for IoT: From technology to application," *Sensors*, vol. 18, no. 11, 2018.
- [3] A. Boulougorgos, P. Diamantoulakis, and G. Karagiannidis, "Low power wide area networks (LPWANS) for Internet of Things (IoT) applications: Research challenges and future trends," *ArXiv e-prints*, Nov. 2016, <https://arxiv.org/abs/1611.07449>.
- [4] O. B. Seller and N. Sornin, "Low power long range transmitter," US Patent 9,252,834, Feb., 2016.
- [5] L. Vangelista, "Frequency shift chirp modulation: The LoRa modulation," *IEEE Signal Processing Letters*, vol. 24, no. 12, pp. 1818–1821, Dec. 2017.
- [6] O. Georgiou and U. Raza, "Low power wide area network analysis: Can LoRa scale?" *IEEE Wireless Communications Letters*, vol. 6, no. 2, pp. 162–165, Apr. 2017.
- [7] M. C. Bor, U. Roedig, T. Voigt, and J. M. Alonso, "Do LoRa low-power wide-area networks scale?" in *ACM International Conference on Modeling, Analysis and Simulation of Wireless and Mobile Systems*, ser. MSWiM '16. New York, NY, USA: ACM, 2016, pp. 59–67.
- [8] M. A. Ben Temim, G. Ferré, B. Laporte-Fauret, D. Dallet, B. Minger, and L. Fuché, "An enhanced receiver to decode superposed LoRa-like signals," *IEEE Internet of Things Journal*, vol. 7, no. 8, pp. 7419–7431, Aug. 2020.
- [9] C. Orfanidis, L. M. Feeney, M. Jacobsson, and P. Gunningberg, "Investigating interference between LoRa and IEEE 802.15.4g networks," in *IEEE International Conference on Wireless and Mobile Computing, Networking and Communications (WiMob)*, Oct. 2017, pp. 1–8.
- [10] L. E. Marquez, A. Osorio, M. Calle, J. C. Velez, A. Serrano, and J. E. Candelo-Becerra, "On the use of LoRaWAN in smart cities: A study with blocking interference," *IEEE Internet of Things Journal*, vol. 7, no. 4, pp. 2806–2815, Apr. 2020.
- [11] T. Voigt, M. Bor, U. Roedig, and J. Alonso, "Mitigating inter-network interference in LoRa networks," in *Proceedings of the 2017 International Conference on Embedded Wireless Systems and Networks (EWSN)*, Feb. 2017.
- [12] J. Haxhibeqiri, F. Van den Abeele, I. Moerman, and J. Hoebeke, "LoRa scalability: A simulation model based on interference measurements," *Sensors*, vol. 17, no. 6, Jun. 2017.
- [13] P. Ferrari, A. Flammini, M. Rizzi, E. Sisinni, and M. Gidlund, "On the evaluation of LoRaWAN virtual channels orthogonality for dense distributed systems," in *IEEE International Workshop on Measurement and Networking (M&N)*, Sep. 2017, pp. 1–6.
- [14] R. Fernandes, R. Oliveira, M. Luís, and S. Sargento, "On the real capacity of LoRa networks: the impact of non-destructive communications," *IEEE Communications Letters*, vol. 23, no. 12, pp. 2437–2441, Dec. 2019.
- [15] D. Croce, M. Gucciardo, I. Tinnirello, D. Garlisi, and S. Mangione, "Impact of spreading factor imperfect orthogonality in LoRa communications," in *Digital Factor Communication. Towards a Smart and Secure Future Internet*, A. Piva, I. Tinnirello, and S. Morosi, Eds. Cham: Springer International Publishing, 2017, pp. 165–179.
- [16] D. Croce, M. Gucciardo, S. Mangione, G. Santaromita, and I. Tinnirello, "Impact of LoRa imperfect orthogonality: Analysis of link-level performance," *IEEE Communications Letters*, vol. 22, no. 4, pp. 796–799, Apr. 2018.
- [17] C. Goursaud and J.-M. Gorce, "Dedicated networks for IoT : PHY / MAC state of the art and challenges," *EAI endorsed trans. on Internet of Things*, Oct. 2015.
- [18] K. Mikhaylov, J. Petäjäjärvi, and J. Janhunen, "On LoRaWAN scalability: Empirical evaluation of susceptibility to inter-network interference," in *2017 European Conference on Networks and Communications (EuCNC)*, Jun. 2017.
- [19] L. Feltrin, C. Buratti, E. Vinciarelli, R. De Bonis, and R. Verdone, "LoRaWAN: Evaluation of link- and system-level performance," *IEEE Internet of Things Journal*, vol. 5, no. 3, pp. 2249–2258, Jun. 2018.
- [20] T. Elshabrawy and J. Robert, "Analysis of BER and coverage performance of LoRa modulation under same spreading factor interference," in *IEEE International Symposium on Personal, Indoor and Mobile Radio Communications (PIMRC)*, Sep. 2018.
- [21] T. Elshabrawy and J. Robert, "Capacity planning of LoRa networks with joint noise-limited and interference-limited coverage considerations," *IEEE Sensors Journal*, pp. 1–1, Feb. 2019.
- [22] A. Mahmood, E. Sisinni, L. Guntupalli, R. Rondón, S. A. Hassan, and M. Gidlund, "Scalability analysis of a LoRa network under imperfect orthogonality," *IEEE Transactions on Industrial Informatics*, vol. 15, no. 3, pp. 1425–1436, Mar. 2019.
- [23] A. Waret, M. Kaneko, A. Guiton, and N. El Rachkidy, "LoRa throughput analysis with imperfect spreading factor orthogonality," *IEEE Wireless Communications Letters*, vol. 8, no. 2, pp. 408–411, Apr. 2019.
- [24] D. Croce, M. Gucciardo, S. Mangione, G. Santaromita, and I. Tinnirello, "LoRa technology demystified: From link behavior to cell-level performance," *IEEE Transactions on Wireless Communications*, vol. 19, no. 2, pp. 822–834, Feb. 2020.
- [25] O. Georgiou, C. Psomas, and I. Krikidis, "Coverage scalability analysis of multi-cell LoRa networks," in *IEEE International Conference on Communications (ICC)*, Jun. 2020, pp. 1–7.
- [26] A. Pop, U. Raza, P. Kulkarni, and M. Sooriyabandara, "Does bidirectional traffic do more harm than good in LoRaWAN based LPWA networks?" in *IEEE Global Communications Conference (GLOBECOM)*, Dec. 2017, pp. 1–6.
- [27] K. Q. Abdelfadeel, D. Zorbas, V. Cionca, and D. Pesch, "FREE – fine-grained scheduling for reliable and energy-efficient data collection in LoRaWAN," *IEEE Internet of Things Journal*, vol. 7, no. 1, pp. 669–683, Jan. 2020.
- [28] G. Callebaut and L. Van der Perre, "Characterization of LoRa point-to-point path-loss: Measurement campaigns and modeling considering

- censored data,” *IEEE Internet of Things Journal*, vol. 7, no. 3, pp. 1910–1918, Mar. 2020.
- [29] F. Van den Abeele, J. Haxhibeqiri, I. Moerman, and J. Hoebeke, “Scalability analysis of large-scale LoRaWAN networks in ns-3,” *IEEE Internet of Things Journal*, vol. 4, no. 6, pp. 2186–2198, Dec. 2017.
- [30] B. Reynders, Q. Wang, and S. Pollin, “A LoRaWAN module for ns-3: Implementation and evaluation,” in *Workshop on ns-3*, ser. WNS3 ’18. New York, NY, USA: ACM, 2018, pp. 61–68.
- [31] B. Reynders, Q. Wang, P. Tuset-Peiro, X. Vilajosana, and S. Pollin, “Improving reliability and scalability of LoRaWANs through lightweight scheduling,” *IEEE Internet of Things Journal*, vol. 5, no. 3, pp. 1830–1842, Jun. 2018.
- [32] D. Magrin, M. Capuzzo, and A. Zanella, “A thorough study of LoRaWAN performance under different parameter settings,” *IEEE Internet of Things Journal*, vol. 7, no. 1, pp. 116–127, Jan. 2020.
- [33] T. To and A. Duda, “Simulation of LoRa in NS-3: Improving LoRa performance with CSMA,” in *2018 IEEE International Conference on Communications (ICC)*, May 2018, pp. 1–7.
- [34] N. Kouvelas, V. Rao, and R. R. V. Prasad, “Employing p-CSMA on a LoRa network simulator,” May 2018.
- [35] M. Slabicki, G. Premsankar, and M. Di Francesco, “Adaptive configuration of LoRa networks for dense IoT deployments,” in *NOMS 2018 - 2018 IEEE/IFIP Network Operations and Management Symposium*, Apr. 2018, pp. 1–9.
- [36] A. M. Yousuf, E. M. Rochester, B. Ousat, and M. Ghaderi, “Throughput, coverage and scalability of LoRa LPWAN for Internet of Things,” in *2018 IEEE/ACM 26th International Symposium on Quality of Service (IWQoS)*, Jun. 2018, pp. 1–10.
- [37] M. Centenaro, L. Vangelista, and R. Kohno, “On the impact of downlink feedback on LoRa performance,” in *IEEE Annual International Symposium on Personal, Indoor, and Mobile Radio Communications (PIMRC)*, Oct. 2017, pp. 1–6.
- [38] J. Finnegan, R. Farrell, and S. Brown, “Analysis and enhancement of the LoRaWAN adaptive data rate scheme,” *IEEE Internet of Things Journal*, vol. 7, no. 8, pp. 7171–7180, Aug. 2020.
- [39] A. Furtado, J. Pacheco, and R. Oliveira, “PHY/MAC uplink performance of LoRa class A networks,” *IEEE Internet of Things Journal*, vol. 7, no. 7, pp. 6528–6538, Jul. 2020.
- [40] B. Reynders, W. Meert, and S. Pollin, “Range and coexistence analysis of long range unlicensed communication,” in *International Conference on Telecommunications (ICT)*, May 2016, pp. 1–6.
- [41] B. Reynders and S. Pollin, “Chirp spread spectrum as a modulation technique for long range communication,” in *2016 Symposium on Communications and Vehicular Technologies (SCVT)*, Nov. 2016.
- [42] T. Elshabrawy and J. Robert, “Closed-form approximation of LoRa modulation BER performance,” *IEEE Communications Letters*, vol. 22, no. 9, pp. 1778–1781, Sep. 2018.
- [43] C. Ferreira Dias, E. Rodrigues de Lima, and G. Fraidenraich, “Bit error rate closed-form expressions for LoRa systems under Nakagami and Rice fading channels,” *Sensors*, vol. 19, Oct 2019.
- [44] G. Baruffa, L. Rugini, V. Mecarelli, L. Germani, and F. Frescura, “Coded LoRa performance in wireless channels,” in *IEEE Annual International Symposium on Personal, Indoor and Mobile Radio Communications (PIMRC)*, Sep. 2019, pp. 1–6.
- [45] J. Courjault, B. Vrigneau, M. Gautier, and O. Berder, “Accurate LoRa Performance evaluation using Marcum function,” in *Globecom 2019*, Dec. 2019. [Online]. Available: <https://hal.archives-ouvertes.fr/hal-02418665>
- [46] O. Afisiadis, A. Burg, and A. Balatsoukas-Stimming, “Coded LoRa frame error rate analysis,” in *IEEE International Conference on Communications (ICC)*, Jun. 2020.
- [47] G. Baruffa, L. Rugini, L. Germani, and F. Frescura, “Error probability performance of chirp modulation in uncoded and coded LoRa systems,” *Elsevier Digital Signal Processing*, vol. 106, Nov. 2020.
- [48] Y. Guo and Z. Liu, “Time-delay-estimation-liked detection algorithm for LoRa signals over multipath channels,” *IEEE Wireless Communications Letters*, vol. 9, no. 7, pp. 1093–1096, Jul. 2020.
- [49] W. Xu, J. Y. Kim, W. Huang, S. S. Kanhere, S. K. Jha, and W. Hu, “Measurement, characterization, and modeling of LoRa technology in multifloor buildings,” *IEEE Internet of Things Journal*, vol. 7, no. 1, pp. 298–310, Jan. 2020.
- [50] O. Afisiadis, M. Cotting, A. Burg, and A. Balatsoukas-Stimming, “On the error rate of the LoRa modulation with interference,” *IEEE Transactions on Wireless Communications*, vol. 19, no. 2, pp. 1292–1304, Feb. 2020.
- [51] T. Elshabrawy, P. Edward, M. Ashour, and J. Robert, “On the different mathematical realizations for the digital synthesis of LoRa-based modulation,” in *European Wireless 2019; 25th European Wireless Conference*, May 2019, pp. 1–6.
- [52] A. Marquet, N. Montavont, and G. Z. Papadopoulos, “Investigating theoretical performance and demodulation techniques for LoRa,” in *IEEE International Symposium on “A World of Wireless, Mobile and Multimedia Networks” (WoWMoM)*, June 2019, pp. 1–6.
- [53] A. Marquet, N. Montavont, and G. Z. Papadopoulos, “Towards an SDR implementation of LoRa: Reverse-engineering, demodulation strategies and assessment over Rayleigh channel,” *Computer Communications*, vol. 153, pp. 595 – 605, 2020.
- [54] T. Elshabrawy and J. Robert, “Interleaved chirp spreading LoRa-based modulation,” *IEEE Internet of Things Journal*, vol. 6, no. 2, pp. 3855–3863, Apr. 2019.
- [55] R. Ghanaatian, O. Afisiadis, M. Cotting, and A. Burg, “LoRa digital receiver analysis and implementation,” in *IEEE International Conference on Acoustics, Speech and Signal Processing (ICASSP)*, May 2019.
- [56] M. Chiani and A. Elzanaty, “On the LoRa modulation for IoT: Waveform properties and spectral analysis,” *IEEE Internet of Things Journal*, vol. 6, no. 5, pp. 8463–8470, Oct. 2019.
- [57] G. K. Karagiannidis and A. S. Lioumpas, “An improved approximation for the Gaussian Q-function,” *IEEE Communications Letters*, vol. 11, no. 8, pp. 644–646, Aug. 2007.
- [58] C. Bernier, F. Dehmas, and N. Deparis, “Low complexity LoRa frame synchronization for ultra-low power software-defined radios,” *IEEE Transactions on Communications*, vol. 68, no. 5, pp. 3140–3152, May 2020.
- [59] M. Xhonneux, D. Bol, and J. Louveaux, “A low-complexity synchronization scheme for LoRa end nodes,” *ArXiv e-prints*, Dec. 2019, <https://arxiv.org/abs/1912.11344>.
- [60] J. Tapparel, O. Afisiadis, P. Mayoraz, A. Balatsoukas-Stimming, and A. Burg, “An open-source LoRa physical layer prototype on GNU radio,” in *International Workshop on Signal Processing Advances in Wireless Communications (SPAWC)*, May 2020, pp. 1–5.